Effect of nanoclay addition on the fiber/matrix adhesion in epoxy/glass composites

Andrea Dorigato, Stefano Morandi and Alessandro Pegoretti

Abstract

Various kinds of organo-modified clays were dispersed at different amounts in an epoxy matrix. After clay addition, the viscosity of the epoxy resin resulted still acceptable for a possible usage as matrices for fiber-reinforced composites. The formation of intercalated microstructures led to substantial improvements of the thermal (glass transition temperature) and mechanical (fracture toughness) properties of the epoxy matrix. E-glass fiber/matrix interfacial shear strength was evaluated by the single-fiber microdebonding method. The introduction of organo-modified clays led to the formation of a stronger fiber-matrix interface, with an increase of the interfacial shear strength of about 30%. Concurrently, the evaluation of the fiber/matrix contact angle revealed an improved wettability when organo-modified clays were added.

Keywords

glass fibers, nanocomposites, fracture toughness, fiber/matrix adhesion

Introduction

Polymeric nanocomposites attracted a wide interest in the recent years, and a large number of papers has been published in the last decade on the thermomechanical properties of nanomodified thermoplastic or thermosetting matrices.[1–5] Among industrially relevant nanofillers, lamellar silicates (montmorillonites) are probably the most investigated.[6,7] These nanofillers are characterized by a lamellar structure, in which crystal lattice consists of two-dimensional layers 1 nm thick and 200–300 nm long, where a central octahedral sheet of alumina or magnesia is alternated to two external silica tetrahedrons. These layers form stacks with a regular van der Waals gap between them. Isomorphic substitution within the layers generates negative charges that are generally counterbalanced by Na^+ or Ca^{2+} cations located in the interlayer galleries. As the forces that hold the stacks together are relatively weak, the intercalation of small molecules between the layers is relatively easy.[8] In order to obtain a more organophilic clay, the hydrated cations of the interlayer can be exchanged with cationic surfactants such as alkylammonium or alkylphosphonium salts,[9–11] thus obtaining so-called organo-modified (OM) clays. Depending on the chemical nature of the modifier and the method

of preparation, three main types of composites may be obtained when OM clays are mixed in a polymer in the liquid state. When the polymer is unable to intercalate between the silicate sheets, a phase-separated microcomposite is formed. Intercalated structure can be obtained when polymer chains are present in the interlayer galleries of the silicate layers, resulting in a well-ordered multilayer morphology built up with alternating polymeric and inorganic layers. When the silicate layers are completely and uniformly dispersed in a continuous polymer matrix, an exfoliated (or delaminated) structure is obtained.[12] The thermomechanical behavior of polymer-clay nanocomposites markedly depend on the dispersion level of the clay in the polymer matrix, which in turn is determined by the filler-matrix interactions.[13]
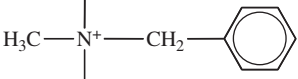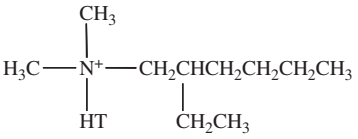
The range of properties where nanoclays are expected to yield improvements over neat polymers is very wide. The advantages due to the use of

Department of Materials Engineering and Industrial Technologies, University of Trento, 38123, Trento, Italy

Corresponding author:
Andrea Dorigato, Department of Materials Engineering and Industrial Technologies, University of Trento, 38123, Trento, Italy
Email: andrea.dorigato@ing.unitn.it

Table 1. Cloisite® clays utilized in this work

Trade Name	Organic modifier	Modifier concentration (meq/100g clay)	Density (g·cm^{-3})	d001 spacing (nm)
Cloisite 30B		90	1.87	1.85
Cloisite 10A		125	1.90	1.92
Cloisite 25A		95	1.87	1.86

T: tallow (~65% C18; ~30% C16; ~5% C14), HT: hydrogenated tallow.
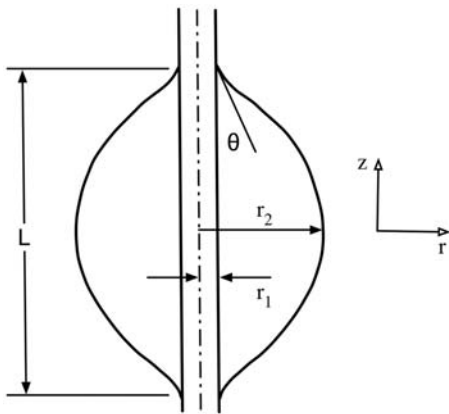
Figure 1. Schematic representation of a matrix drop deposited on a rigid fiber.

nanocomposites are generally manifested in terms of improvements of the quasi-static tensile mechanical properties[14–17] and of the fracture resistance,[18–21] in an increase of the dimensional stability[22] and of the barrier properties,[23] in a better thermal degradation resistance.[24,25] Nevertheless, the mechanical properties obtained so far with polymer nanocomposites are much lower than those typically required to engineering structural materials, such as advanced composites reinforced with high-performance continuous fibers.[26] In recent years, a rising interest emerged for the development of ternary composites in which both traditional
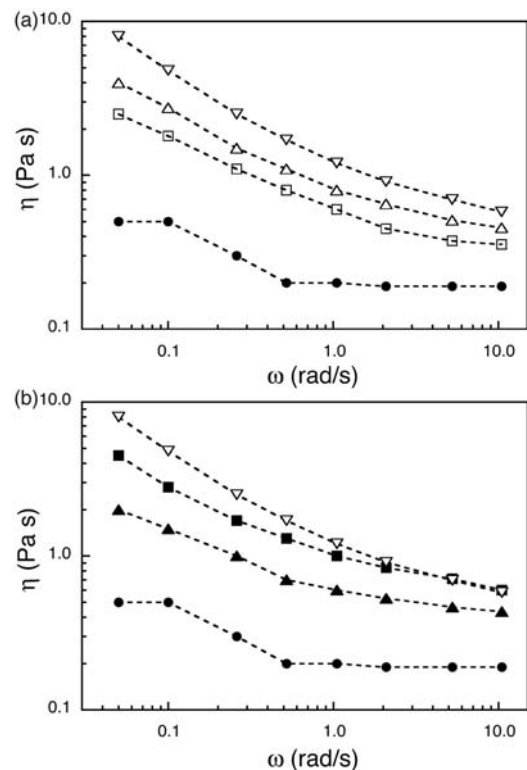
Figure 2. Viscosity measurements on epoxy clay nanocomposites. (a) Effect of the filler content, (●) Epoxy, (□) Epoxy-10A-1, (△) Epoxy-10A-3, (▽) Epoxy-10A-5. (b) Effect of the clay type, (●) Epoxy, (■) Epoxy-30B-5, (▽) Epoxy-10A-5, (▲) Epoxy-25A-5.

continuous high-strength micro-fibers and nanofillers are concurrently added to a thermosetting[27–30] or a thermoplastic polymer matrix.[31,32] In particular, some attempts have been made to improve the matrix-dominated properties of polymer composites by adding OM clays to the epoxy matrix.

Despite the large number of publications on epoxy-clay nanocomposites, the effect of the nanoclay addition on the interfacial adhesion properties of epoxy matrices in contact with traditional high-strength fibers such as glass, carbon, kevlar, etc. was not investigated to the best of our knowledge.

In this work, epoxy/clay nanocomposites were prepared by using three different kinds of OM clays. A microstructural analysis was conducted, in order to determine the role of clay hydrophobicity on its dispersion in the epoxy matrix. The mechanical behavior was then analyzed, in order to determine the role of the polymer-filler interaction on the quasi-static properties and on the fracture resistance of the resulting materials. Finally, a detailed study of E-glass fiber-matrix adhesion was carried out, through microdebonding tests and contact angle measurements. This kind of information is of primary importance for the development of nano-modified glass fiber-reinforced structural composites, with improved interlaminar resistance.

Experimental section

A bi-component epoxy resin, supplied by Elantas Camattini (Collecchio, Italy), was selected as polymer matrix. An EC157 epoxy base (density at $25°C = 1.15$ g cm^{-3}, viscosity at $25°C = 700$ mPa s), constituted by a mixture of Bisphenol A/Bisphenol F/Hexanediol diglycidyl ether (equivalent epoxide weight [EEW] = 165–180 g·equiv^{-1}), was mixed with a W152 LR amminic hardener (density at $25°C = 0.95$ g·cm^{-3}, viscosity at 25 °C = 30 mPa·s) at a weight ratio of 100/30. The rheological and mechanical properties of this resin are suitable for its usage in the preparation of high-performance composites through resin infusion or vacuum-assisted resin transfer moulding (VARTM) processes.

Three different OM clays (Cloisite® 30B, 10A, and 25A), provided by Southern Clay Products, Inc. (Gonzales, Texas), were used. Table 1 summarizes some of the characteristics of the selected organoclays. According to the producer's selection chart and to a previous investigation of this research group,[13] the selected organoclays can be ranked in the following order of increasing hydrophobicity: 30B < 10A < 25A. Both the resin and the clays were utilized as received.

For as concerns the preparation of the samples, the clays were added to the epoxy base and the mixture mechanically mixed for 1 h in a Dispermat® F1 mixer operating at 2000 rpm. The mixture was then ultrasonicated for 5 min at 260 W·cm^{-2} through a Hielscher® 400S sonicator equipped with a sonotrode of a diameter of 14 mm, and then degassed at ambient temperature. The hardener was then added and mechanically mixed by a Dispermat® F1 mixer for 5 min at 500 rpm. Finally, the mixture was degassed again at ambient temperature and poured in the cavities of a silicone mould. A curing cycle of 2 h at 50°C followed by 2 h at 80°C was then conducted. According to this procedure, pure epoxy samples and nanocomposites filled with different clays at various filler contents (1 wt%, 3 wt%, and 5 wt%) were prepared. The samples were denoted indicating the matrix (Epoxy) and the kind of clay (30B, 10A, or 25A), followed by the filler content. As a title of example, the 5 wt% Cloisite 25A-filled nanocomposite is indicated as Epoxy-25A-5.

Rheological measurements were conducted on pure epoxy and nanofilled mixtures before curing in a Brookfield RVT coaxial viscosimeter, with an inner diameter of 17 mm and an outer diameter of 19 mm, in a shear rate interval between 0.05 and 10.5 rad·s^{-1}. For each composition, a sample volume of 8 mL was poured between the cylinders and tested at a temperature of 25°C controlled by a thermostatic chamber.

X-Ray diffraction (XRD) analysis was conducted on fully cured nanofilled samples, in order to evaluate the dispersion level of the organoclays. A Laue diffractometer, with a non-monochromatized copper radiation of 0.15406 nm wavelength, was utilized both in transmission and in reflection geometry. By utilizing the Bragg's Law, the interlamellar distances of the clay powder (d_0) and of the clays in the composites (d) was evaluated. According to a previous work of this research group on polyurethane-clay nanocomposites,[13] the intercalation degree (ID), representing the increase of the d-spacing with respect to the original interlamellar distance of the clay, was determined as follows:

$$ID = \frac{d - d_0}{d_0} \qquad (1)$$

Dynamical mechanical thermal analysis (DMTA) was conducted by using an MKII Polymer Laboratories machine. Rectangular samples, 25-mm long, 4-mm thick, and 5-mm wide, were tested in tensile conditions, in a temperature interval between 0°C and 160°C, at an heating rate of 3 K·min^{-1}. A sinusoidal strain with an amplitude of 64 μm (maximum strain = 0.004 mm·mm^{-1}) and a frequency of 1 Hz was imposed. In this way, the temperature dependence of storage modulus (E') and of the loss factor (tanδ) values were determined. The glass transition temperature (T_g) was evaluated as the peak of the tanδ curves.

Quasi-static tensile properties were determined by using an Instron 4502 electromechanical tensile testing machine, at a crosshead speed of 1 mm·min^{-1}. ISO-527 dogbone samples, with a gage length of 50 mm, a width of 10 mm, and a thickness of 4 mm, were tested. The axial deformation was evaluated through an Instron 2620–601 extensometer, with a gage length of 12.5 mm. According to ISO 527 standard, the elastic modulus (E) was calculated as a secant modulus between the strain levels of 0.05% and of 0.25%. All tests were conducted at ambient temperature (23°C), and at least five specimens were tested for each sample.

According to ASTM D 5045 standard, plane strain fracture toughness parameter (K_{IC}) was evaluated on single edge notched bend (SENB) specimens (44 mm long, 10 mm wide, and 4 mm thick) containing a sharp notch produced by a razor blade (radius of 0.01 mm), about 5 mm deep. A crosshead speed of 10 mm·min^{-1} was adopted in the three-point bending tests and at least five specimens were tested for each sample.

Fracture surfaces of SENB specimens were observed at various magnifications by a Zeiss Supra 40 field emission scanning electronic microscope (FESEM), at an acceleration voltage of 10 kV and a pressure of 10^{-6} Torr.

In order to evaluate the effect of the clay addition on the fiber-matrix interfacial adhesion, single fiber microdebonding tests were performed. Single fibers were randomly extracted from an E-glass woven fabric (areal weight 380 g·m^{-2}) surface treated with a proprietary epoxy compatible sizing and kindly supplied by Angeloni SpA (Venice, Italy). The fibers had an average diameter of about 19.8 ± 1.6 μm. The deposition of the resin microdrops (mean diameter of about 80 μm) on the fibers was conducted under a Wild Heerbrugg MGD17 optical microscope. The drops were picked up on the tip of a thicker glass filament and deposited on the fibers supported on paper frames. The drops were then cured with the same curing cycle utilized for the dogbone samples, that is, 2 h at 50°C followed by 2 h at 80°C. Microdebonding tests were conducted at a crosshead speed of 1 mm·min^{-1} by an Instron 4502 tensile testing machine equipped with a 10 N load cell. The brackets of the microdebonding device were positioned with a gap of 24 μm and at least 10 specimens were tested for each sample. A nominal interfacial shear stress (τ) was computed by using the following expression:

$$\tau = \frac{F}{\pi dL} \tag{2}$$

where F is the load registered during the test, d is the fiber diameter, and L is the length of the drop. When a critical load is reached, the fiber-matrix interface fails and the load abruptly decreases. If the maximum load is inserted in Equation (2), an interfacial shear strength (ISS) can be estimated. Before and after the microdebonding test, single fiber specimens were observed through a Philips XL30 environmental scanning electron microscope (ESEM), at an acceleration voltage of 4.5 keV and a pressure of 0.7 Torr.

Fiber-matrix contact angles were also evaluated on the microdebonding specimens following an approach proposed by Carroll.[33] As schematically represented in Figure 1, it is supposed that the drop assumes a symmetric elliptical shape around the fiber. Neglecting the effect of gravity force, the shape of the fiber is governed by the Laplace equation:

$$-\frac{dr}{dz} = \frac{\left[(r_2^2 - r^2)(r^2 - a^2 r_1^2)\right]^{1/2}}{r^2 + a r_1 r_2} \tag{3a}$$

where

$$a = \frac{r_2 \cos\theta - r_1}{r_2 - r_1 \cos\theta} \tag{3b}$$

and r_1 is the fiber radius, r_2 is the maximum radius of the drop, θ is the contact angle, and r and z represent the radial and the longitudinal directions, respectively. By measuring r_1 and r_2 with an optical microscope and integrating along the length L with an iterative procedure, the fiber-matrix contact angle θ can be evaluated on the basis of Equations (3a) and (3b). A minimum of five microdrops were analyzed for each sample.

Results and discussions

Rheological characterization

Shear rate-dependent viscosity (η) values of pure epoxy and relative nanocomposite mixtures are reported in Figure 2. The introduction of the clay in these systems leads to a viscosity increase proportional to the filler content, as clearly evident in Figure 2(a) where the rheological curves of pure epoxy and relative nanocomposites containing various amounts of Cloisite 10 A OM clay are compared. The viscosity enhancement is more pronounced in the low shear rate region, with the disappearance of the pseudo-plastic plateau (solid-like behavior), while viscosity values at high shear rates approach those of pure epoxy. These observations are in agreement with the literature information on the rheological behavior of nanofilled polymeric systems.[34–38] According to the observations of Cassagnau,[34] in clay-filled polymeric nanocomposites, the viscosity
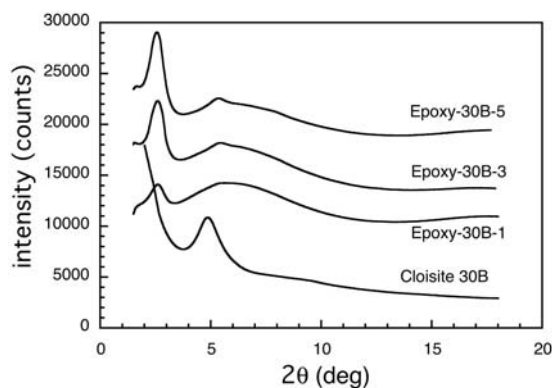
Figure 3. X-Ray scattering patterns for Cloisite 30B powder and Epoxy-30B-x nanocomposites.

Table 2. d and d_0 spacing as revealed from X-Ray diffraction (XRD) measurements

Sample	d_0 (nm)	d (nm)	ID (%)
Epoxy-30B-1	1.79	3.33	86.1
Epoxy-30B-3	1.79	3.41	90.0
Epoxy-30B-5	1.79	3.39	88.9
Epoxy-10A-1	1.90	2.93	54.4
Epoxy-10A-3	1.90	2.93	54.4
Epoxy-10A-5	1.90	2.98	57.1
Epoxy-25A-1	1.93	2.86	48.0
Epoxy-25A-3	1.93	2.85	47.9
Epoxy-25A-5	1.93	2.83	46.8

increase at low frequencies is mainly related to the interactions between clay layers and polymeric matrix, while in fumed metal oxides nanocomposites the solids-like behavior is generally due to particle–particle interactions and the consequent formation of a network structure. At elevated test frequencies, the shear forces are more intensive due to the limited stress relaxation time. Consequently, these interparticle bonds can be destroyed by shear forces, and the viscosity begins to drop down to values comparable to that of the unfilled matrix. In Figure 2(b), the rheological behavior of nanocomposites filled with the same content of various OM clays is compared. It is evident that the highest viscosity values are obtained for Cloisite 10A nanocomposites. This result indicates strong polymer/filler interactions and can be considered as an indirect indication of a good dispersion of this type of clay in the epoxy matrix.

The viscosity of the resin for vacuum-assisted infusion process of large structural components, such as wind rotor blades and a long boat hulls, is usually limited to 100–500 mPa·s,[39] even if values up to 1000 mPa·s are still acceptable. Therefore, considering the typical shear rates involved in the resin infusion process,[40] it is possible to assert that the introduction of the OM clays in concentration up to 5 wt% does not compromise a possible usage of this epoxy resin for infusion processes, as recently experimentally verified.[41]

Microstructural characterization

Representative X-Ray patterns of Cloisite 30B powder and Epoxy-30B-x nanocomposites are reported in Figure 3, while in Table 2 the most relevant parameters are summarized. In the case of 30B-filled systems, it is evident a shift of the diffraction peak to lower angles (about 2.7 deg), irrespectively to the filler content. It can be concluded that all the prepared nanocomposites are characterized by an intercalated structure, with an increase of the interlamellar spacing with respect of the original clay powders. Even if a complete exfoliation of the clay lamellae is reported,[42] the formation of an intercalated structure is more frequently reported in the existing literature on epoxy-clay nanocomposites.[19, 43–48] The ID is slightly higher for the most hydrophilic clay (30B), but the final d-spacing is not substantially influenced by the clay type, passing from 3.4 nm for Epoxy-30B-x composites to 2.9 nm for Epoxy-25A-x samples. Regardless of the filler content, a small percentage of nonintercalated clay, that could negatively affect the mechanical behavior of the resulting composites, can be detected. Of course, XRD analysis is not sufficient by itself to evaluate the influence of the clay typology on the microstructure of the composites, and additional indications, obtained from different experimental techniques, are required to assess the role of the clay hydrophobicity on the microstructure of the prepared composites.

In Figure 4, FESEM images of fracture surfaces of pure epoxy and relative nanocomposites are reported. It is immediately evident that the morphology of the fracture surfaces is heavily affected by the addition of OM clays. In fact, while the pure epoxy sample is very smooth, nanofilled samples display highly corrugated surfaces. Moreover, the surface corrugation appears to be more and more pronounced as the filler content increases (Figure 4(b), (c), and (d)). The corrugation of the fracture surface due to the presence of clay nanoplatelets has been widely reported in the scientific literature,[19,44,49] and the creation of a high amount of fracture surface is generally considered to play a positive role on the fracture toughness of the material. According to the extensive characterization performed by Kinloch and Taylor on the fracture toughness epoxy-based nanocomposites,[50] it can be also hypothesized that the improved fracture performance of nanomodified epoxy may be due to the combination of crack deflection by the silicate nanoplatelets and plastic
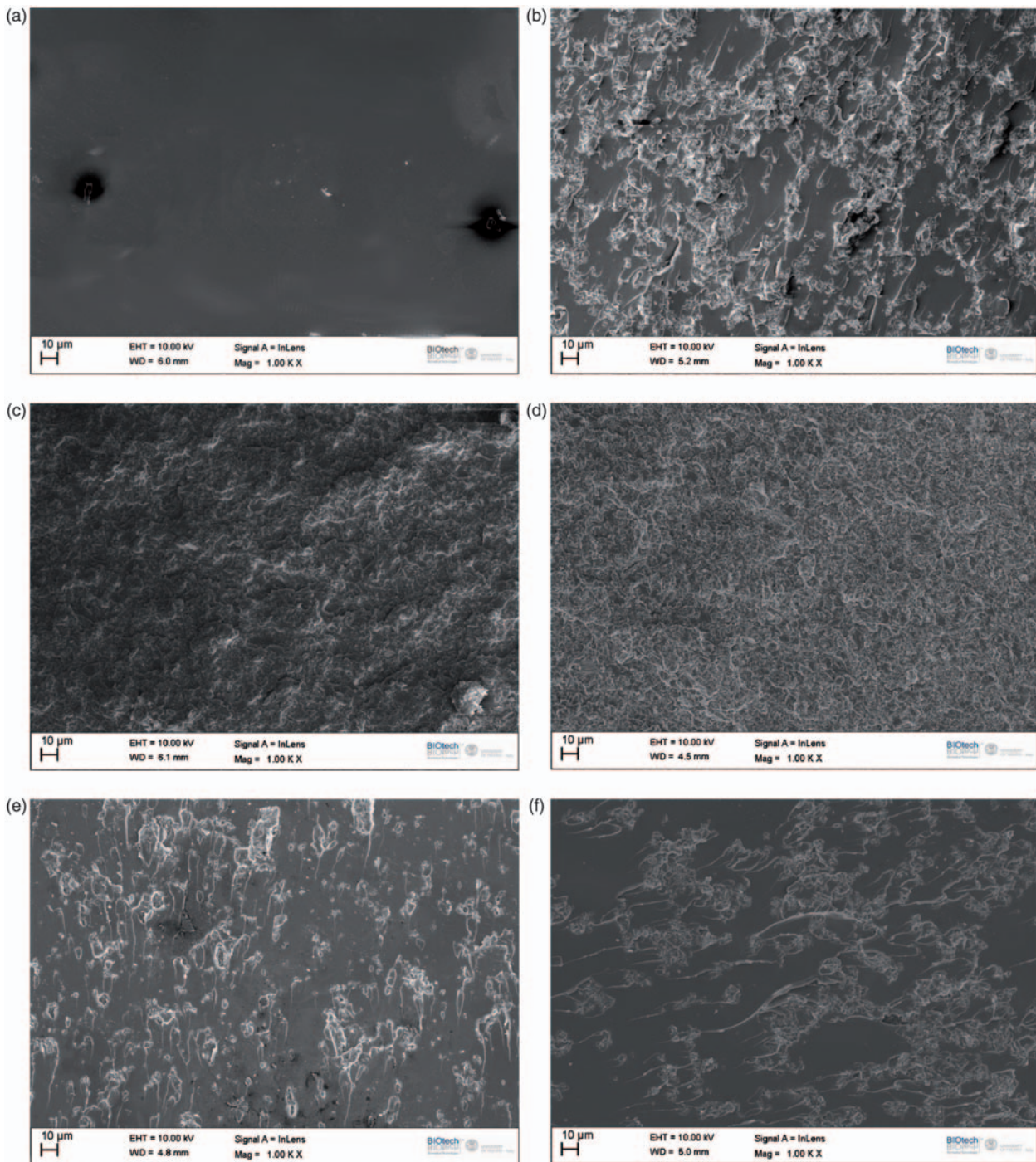
Figure 4. Field emission scanning electronic microscope (FESEM) images of fracture surfaces of epoxy-clay nanocomposites. (a) Epoxy, (b) Epoxy-10A-1, (c) Epoxy-10A-3, (d) Epoxy-10A-5, (e) Epoxy-30B-1, and (f) Epoxy 25A-1.
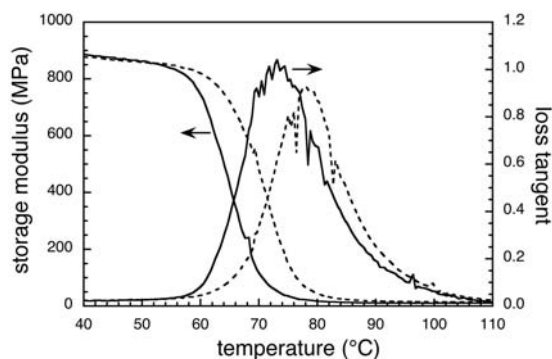
Figure 5. Storage modulus and loss tangent curves of (—) Epoxy and (- - -) Epoxy-10A-5 samples.
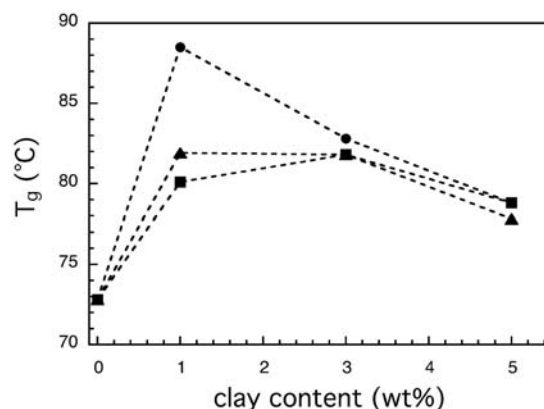

Figure 6. Glass transition temperature of (●) Epoxy-30B-x, (■) Epoxy-10A-x, and (▲) Epoxy-25A-x samples (x = 1 − 5 wt%).

Table 3. Quasi-static tensile properties of epoxy-clay nanocomposites

Clay content (%)	Epoxy-30B-x	Epoxy-10A-x	Epoxy-25A-x
E (GPa)			
0	3.23 ± 0.08		
1	3.15 ± 0.15	3.38 ± 0.09	3.09 ± 0.18
3	3.10 ± 0.10	3.00 ± 0.15	3.18 ± 0.18
5	3.50 ± 0.16	3.15 ± 0.05	3.10 ± 0.22
σ_b (MPa)			
0	69.8 ± 2.0		
1	59.8 ± 6.2	57.3 ± 3.3	53.4 ± 2.9
3	50.5 ± 2.7	49.7 ± 1.6	38.2 ± 2.2
5	46.0 ± 2.4	47.4 ± 0.7	41.1 ± 3.8
ϵ_b (%)			
0	5.9 ± 0.8		
1	3.5 ± 0.7	3.7 ± 0.3	3.6 ± 0.5
3	2.8 ± 0.3	3.1 ± 0.2	2.1 ± 0.3
5	2.3 ± 0.6	2.7 ± 0.1	2.6 ± 0.3

deformation of the matrix around the clay lamellae. The plastic deformation initiates by the matrix debonding from the nanoplatelets, due to the relatively poor adhesion, thus relieving the triaxial constraint at the crack tip and allowing the plastic deformation of the surrounding epoxy matrix. Furthermore, if nanocomposites filled with different clays at the same filler loading are compared (Figure 4(b), (e), and (f)), it can be easily noticed that for Cloisite 10A-filled nanocomposites a more pronounced surface roughness can be observed. This is another indication that Cloisite 10A clay lamellae are probably better dispersed in the epoxy resin with respect to Cloisite 30B and to Cloisite 25A.

Thermomechanical characterization

In Figure 5, representative DMTA storage modulus (E') and loss tangent (tanδ) curves of pure epoxy and Epoxy-10A-5 nanocomposite are compared. While in the temperature region below the glass transition temperature the effect of the introduction of the clay on E' is practically negligible, at temperatures higher than T_g it is possible to detect a substantial enhancement of the storage modulus for the filled sample, probably due to a chain-blocking mechanism promoted by polymer-clay physical interactions. The chain-blocking effect provided by the layered silicate is also responsible of the

lowering of tanδ values and of the shift of its peak at higher temperatures. From this plots, it is also evident that the glass transition temperature increases due to the introduction of the nanoclay, confirming the observations reported by Dean et al. on the chemorheological behavior of epoxy-layered silicate nanocomposites.[47] As evidenced in Figure 6, the maximum T_g increment occurs for a filler content of 1 wt%, while for higher clay contents the glass transition temperature starts to decrease. As previously reported for polyurethane-clay nanocomposites,[13] it is possible that even in this case the occurrence of two concurrent and opposite phenomena is responsible of the observed T_g trend. In fact, as the filler content increases the chain blocking (stiffening) effect is likely to increase and, at the same time, polymer-filler chemical interactions can hinder the cross-linking process of the matrix, with a consequent reduction of its T_g.

Quasi-static tensile properties of pure epoxy and relative nanocomposites are summarized in Table 3. In agreement with DMTA tests, the introduction of OM clays does not substantially affect the elastic modulus at ambient temperature. On the other hand, tensile ultimate properties (i.e. stress, σ_b, and strain, ϵ_b, at break) decrease as the clay content increases. According to some literature explanation,[14,44,51] we believe that the presence of a fraction of nonintercalated clay tactoids with micrometric dimension (see XRD tests) may act as crack nucleation sites, with detrimental effects on the tensile properties at break.

A completely different trend was observed when mechanical tests on notched specimens were conducted for the fracture toughness evaluation. In Figure 7, representative load-displacement curves of pure epoxy and 5 wt% 10A filled nanocomposite obtained from flexural tests on SENB samples are compared, while the resulting K_{IC} values are summarized in Table 4. An increase of K_{IC} with the filler content can be generally observed for the nanofilled samples. It is worthwhile to note that comparable increments of the fracture toughness have been already reported in the scientific literature on epoxy-based nanocomposites.[19,52,53] If in quasi-static tensile tests on un-notched samples the presence of clay aggregates is responsible for the stress concentration and the crack nucleation, it could be hypothesized that, when a notch is already present on the sample, the embrittling effect due to agglomerates is no longer effective, and clay nanoplatelets can render the crack propagation path more tortuous, with a positive contribution on the fracture toughness of the material. Even for fracture toughness, the best performances are those of the nanocomposites filled with Cloisite10A OM clays, probably because of their better dispersion degree, that is also responsible for a higher roughness of the fracture surface (see Figure 4).
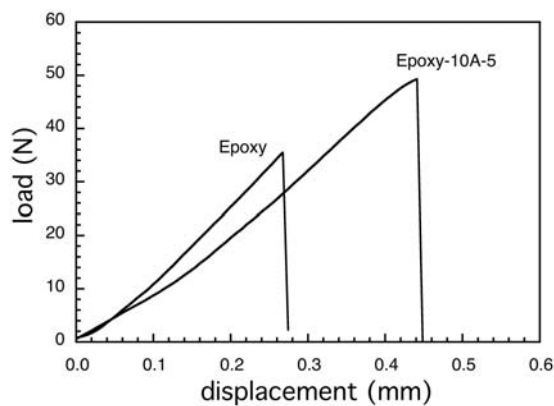
Evaluation of the fiber-matrix adhesion

The positive effect of nanocomposite coatings containing carbon nanotubes (CNTs) and/or nanoclays for healing surface defects of glass fibers and improving interfacial adhesion has been recently assessed by Gao et al.[54] Fiber–matrix adhesion in glass-fiber-reinforced polyamide-6 silicate nanocomposites has been also investigated by Vlasveld and coworkers.[55] By using the single-fiber fragmentaton test, they concluded that

Figure 7. Representative force-displacement curves of Epoxy and Epoxy-10A-5 single edge notched bend (SENB) specimens tested for the determination of K_{IC} values.

Table 4. K_{IC} values of epoxy-clay nanocomposites

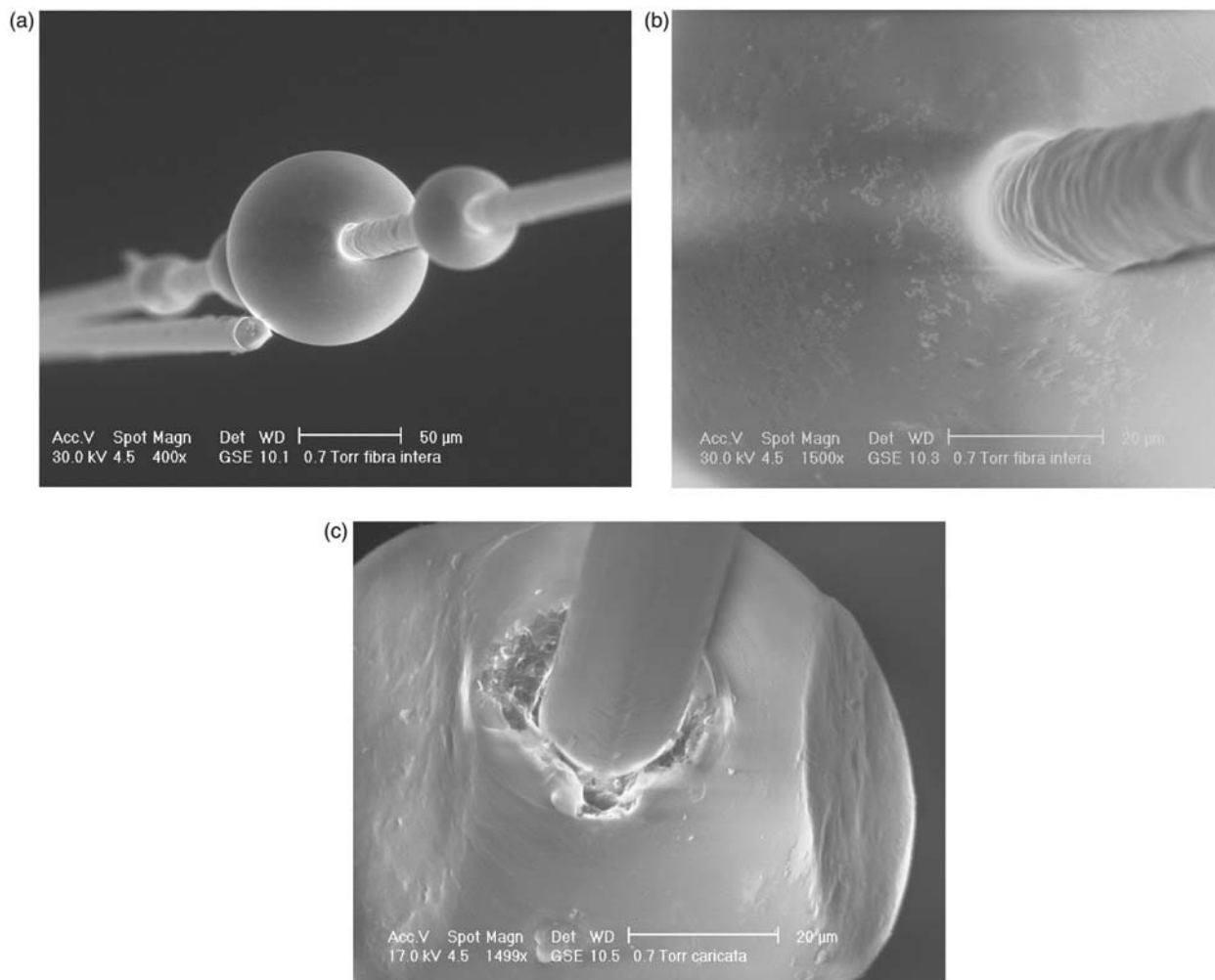| K_{IC} (MPa m$^{0.5}$)			
Clay content (%)	Epoxy-30B-x	Epoxy-10A-x	Epoxy-25A-x
0	0.90 ± 0.08		
1	1.04 ± 0.13	1.06 ± 0.05	1.04 ± 0.06
3	0.97 ± 0.07	1.00 ± 0.05	1.07 ± 0.05
5	1.02 ± 0.06	1.26 ± 0.07	1.10 ± 0.04

Figure 8. Environmental scanning electron microscope (ESEM) images of (a) pure epoxy drop on a glass fiber for the microdebonding tests, (b) detail of the fiber-drop interface before microdebonding, (c) detail of the fiber-drop interface after debonding.
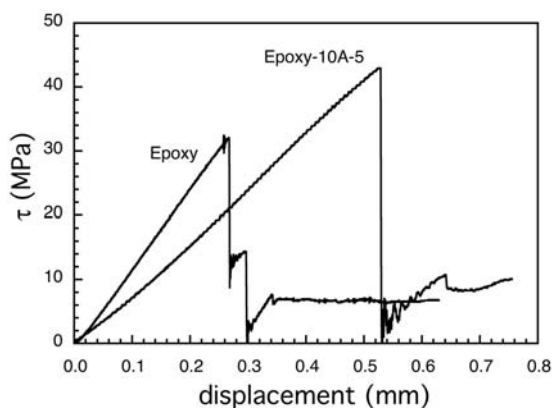

Figure 9. Representative interfacial shear stress-displacement curves registered in microdebonding tests with Epoxy and Epoxy-10A-5 drops.
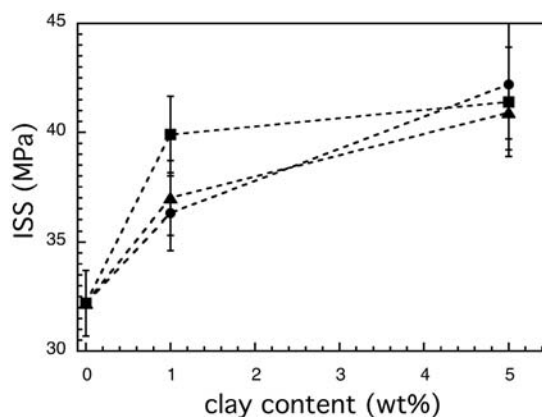

Figure 10. Interfacial shear strength values as a function of clay content and type in the epoxy drops: (●) Epoxy-30B-*x*, (■) Epoxy-10A-*x*, and (▲) Epoxy-25A-*x* (*x* = 1 − 5 wt%).
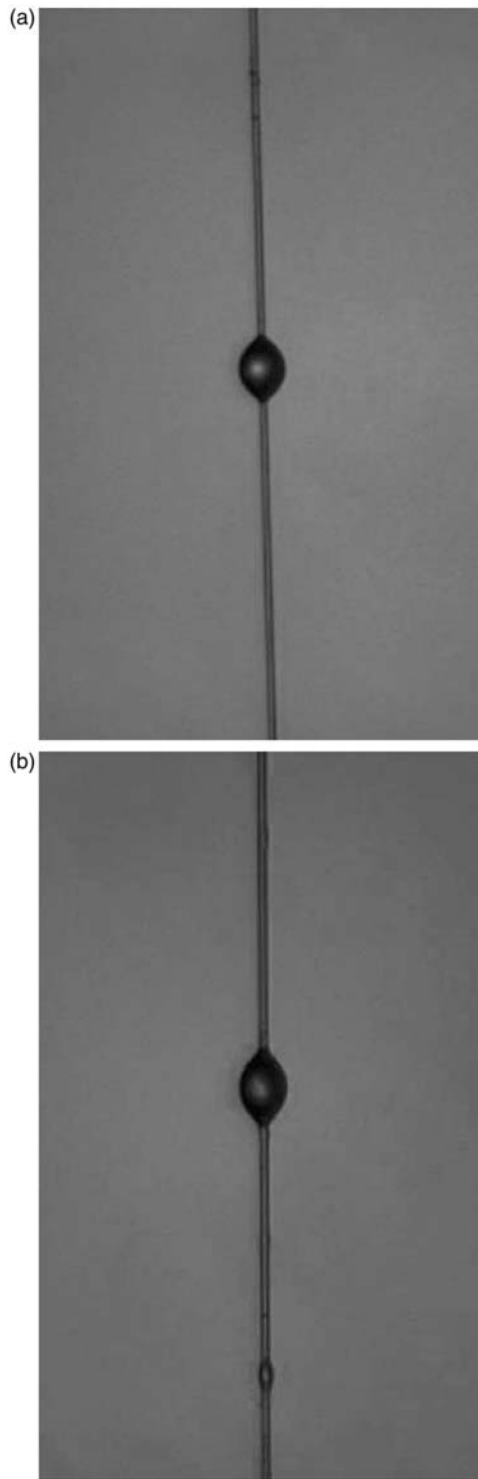
Figure 11. Optical microscope images of (a) pure epoxy drop and of (b) Epoxy-25A-5 drop on a glass fiber.

the failure mechanism is by interfacial de-bonding and that the addition of nanoparticles has a negative effect on the bonding between the matrix and the glass fibers. Interfacial evaluation of glass fiber reinforced – CNTs – epoxy ternary composites and the hydrophobicity of CNT-epoxy nanocomposites were recently investigated by micromechanical and wettability tests by Park et al.[56] The authors reported an improvement of the interfacial shear strength between the etched glass fiber and the CNT-epoxy nanocomposites attributed to an enhanced surface energy and roughness. To the best of our knowledge, no information is currently available in the scientific literature on the effect on the fiber-matrix interfacial properties of OM clays homogenously dispersed in epoxy resin.

In Figure 8(a), an ESEM image of a microdebonding single fiber specimen is reported in which an epoxy drop is deposited onto a glass fiber. Magnifications of the fiber-drop interface before and after the microde-bonding test are reported in Figures 8(b) and (c), respectively. It is worthwhile to note that the drop is perfectly centred around the fiber, while in Figure 8(c) is evident the fracture zone around the fiber and the deformation imposed on the resin drop by the micro-wises of the testing device.

In Figure 9, representative interfacial shear stress (τ) vs. displacement curves registered in microdebonding tests for Epoxy and Epoxy-10A-5 nanocomposite are reported. It is evident that the addition of OM clay induces a substantial increase of the fiber-matrix load transfer ability of the epoxy matrix. Interfacial shear strength values of pure epoxy and relative nanocomposites drops on E-glass fibers are summarized in Figure 10. It can be observed that the introduction of OM clays in this epoxy system leads to a remarkable increase of the interfacial resistance, which is proportional to the filler content and apparently independent from the clay type. In order to better understand the reasons behind this result, fiber-epoxy drop contact angles were determined by optical measurements of the parameters involved in the Laplace equation (see Equations (3a) and (3b)). In Figure 11, optical micro-scope images of an Epoxy drop and of an Epoxy-25A-5 drop on a glass fiber are represented, while in Table 5 contact angle values for all the tested samples are sum-marized. It clearly emerges that as a consequence of the addition of OM clays is a reduction of the contact angle values, that is, a better fiber-matrix wettability. Even in this case, the effect is apparently independent from the clay content and only slightly affected by the clay type. The positive contribution of the clay presence on the adhesion mechanisms can therefore be advocated to explain the enhancements of the interlaminar crack propagation resistance experimentally reported in some paper on ternary nanoclay modified epoxy-glass

Table 5. Fiber-epoxy drop contact angle.

Contact angle (deg)			
Clay content (%)	Epoxy-30B-x	Epoxy-10A-x	Epoxy-25A-x
0	22.6 ± 4.0		
1	16.9 ± 4.5	18.1 ± 4.8	14.4 ± 3.0
5	16.7 ± 3.4	18.1 ± 4.0	13.2 ± 4.1

fiber-reinforced composites[57,58] and can be an important basis for the design of novel structural composites, with improved inter- or translaminar fracture resistance.

Conclusions

Epoxy-clay nanocomposites were prepared by using various types of OM clays, in order to evaluate their potential use as matrices for structural long-fiber composites with improved properties.

Rheological measurements revealed that the viscosity enhancement due to the presence of clay lamellae is proportional to the filler content and compatible with the technological limits imposed by the traditional resin infusion process. XRD analysis evidenced the formation of an intercalated structure for all the samples, even if from rheological tests and fracture surface analysis is probable that Cloisite 10A-filled samples were characterized by the best dispersion degree. Fracture toughness was substantially improved by the clay addition, especially in the case of 5 wt% Cloisite 10A-filled sample. The investigation of the fiber-matrix interfacial adhesion through the single-fiber microdebonding tests revealed a marked (about +30%) increase of the interfacial shear strength for the nanofilled samples. Concurrently, a lowering of the fiber-matrix contact angle values has been observed when the OM clays were added to the epoxy resin. The enhanced interfacial adhesion and the improved fiber-matrix wettability could be important for the production of nanomodified structural composites with improved interlaminar resistance.

References

1. Paul DR and Robeson LM. Polymer nanotechnology: Nanocomposites. *Polymer* 2008; 49(15): 3187–204.
2. Pavlidou S and Papaspyrides CD. A review on polymer-layered silicate nanocomposites. *Progr Polymer Sci* 2008; 33(12): 1119–1198.
3. Bondioli F, Dorigato A, Fabbri P, Messori M and Pegoretti A. High-density polyethylene reinforced with submicron titania particles. *Polymer Eng Sci* 2008; 48: 448–457.
4. Bondioli F, Dorigato A, Fabbri P, Messori M and Pegoretti A. Improving the creep stability of high-density polyethylene with acicular titania nanoparticles. *J Appl Polymer Sci* 2009; 112: 1045–1055.
5. Dorigato A, Pegoretti A and Migliaresi C. Physical properties of polyhedral oligomeric silsesquioxanes–cycloolefin copolymer nanocomposites. *J Appl Polymer Sci* 2009; 114: 2270–2279.
6. Alexandre M and Dubois P. Polymer-layered silicate nanocomposites: Preparation, propertiesand uses of a new class of materials. *Mater Sci Eng R Rep* 2000; 28: 1–63.
7. Giannelis EP, Krishnamoorti R and Manias E. Polymer-silica nanocomposites: Model systems for confined polymers and polymer brushes. *Adv Polymer Sci* 1999; 118: 108–147.
8. Theng BKG. *The chemistry of clay-organic reactions*. London: Adam Hilger Ltd, 1974.
9. Kovarova L, Kalendova A, Gerard JF, Malac J, Simonik J and Weiss Z. Structure analysis of PVC nanocomposites. *Macromol Symp* 2005; 221: 105–114.
10. Peprnicek T, Duchet J, Kovarova L, Malac J, Gerard JF and Simonik J. Polyvinylchloride/clay nanocomposites : X-ray diffraction, thermal and rheological behaviour. *Polymer Degrad Stabil* 2006; 91: 1855–1860.
11. Peprnicek T, Kalendova A, Pavlova E, Simonik J, Duchet J and Gerard JF. Polyvinylchloride-paste/clay nanocomposites: Investigation of thermal and morphological characteristics. *Polymer Degrad Stabil* 2006; 91: 3322–3329.
12. Song Hu Y, Tang Y, Zhang R, Chen R and Fan W. Study on the properties of flame retardant polyurethane/organoclay nanocomposite. *Polymer Degrad Stabil* 2005; 87: 111–116.
13. Pegoretti A, Dorigato A, Brugnara M and Penati A. Contact angle measurements as a tool to investigate the filler–matrix interactions in polyurethane–clay nanocomposites from blocked prepolymer. *Eur Polymer J* 2008; 44: 1662–1672.

14. Isik I, Yilmazer U and Bayram G. Impact modified epoxy/montmorillonite nanocomposites: Synthesis and characterization. *Polymer* 2003; 44: 6371–6377.

15. Lin JC, Chang LC, Nien MH and Ho HL. Mechanical behaviour of various nanoparticle filled composites at low-velocity impact. *Compos Struct* 2006; 74(1): 30–36.

16. Dorigato A, Fambri L, Pegoretti A, Slouf M and Kolarik J. Cycloolefin copolymer (COC)/fumed silica nanocomposites. *J Appl Polymer Sci* 2011; 119: 3393–3402.

17. Dorigato A and Pegoretti A. Tensile creep behaviour of poly(methylpentene)-silica nanocomposites. *Polymer Int* 2010; 59: 719–724.

18. Avlar S and Qiao Y. Effects of cooling rate on fracture resistance of nylon 6-silicate nanocomposites. *Compos A* 2005; 36(5): 624–630.

19. Liu W, Ho SV and Pugh M. Fracture toughness and water uptake of high-performance epoxy/nanoclay nanocomposites. *Compos Sci Technol* 2005; 65: 2364–2673.

20. Ragosta G, Abbate M, Musto P, Scarinzi G and Mascia L. Epoxy-silica particulate nanocomposites: Chemical interactions, reinforcement and fracture toughness. *Polymer* 2005; 46(23): 10506–10516.

21. Yao XF, Yeh HY and Zhao HP. Dynamic response and fracture characterization of polymer–clay nanocomposites with Mode-I Crack. *J Compos Mater* 2005; 39(16): 1487–1496.

22. Dorigato A, Pegoretti A and Kolarik J. Nonlinear tensile creep of linear low density polyethylene/fumed silica nanocomposites : Time-strain superposition and creep prediction. *Polymer Compos* 2010; 31: 1947–1955.

23. Kim JK, Hu C, Woo RSC and Sham ML. Moisture barrier characteristics of organoclay–epoxy nanocomposites. *Compos Sci Technol* 2005; 65: 805–813.

24. Varghese S, Gatos KG, Apostolov AA and Karger-Kocsis J. Morphology and mechanical properties of layered silicate reinforced natural and polyurethane rubber blends produced by latex compounding. *J Appl Polymer Sci* 2004; 92: 543–551.

25. Zhang J, Jiang DD and Wilkie CA. Fire properties of styrenic polymer–clay nanocomposites based on oligomerically-modified clay. *Polymer Degrad Stabil* 2005; 91(2): 358–366.

26. Dzenis Y. Materials science‐structural nanocomposites. *Science* 2008; 319(5862): 419–420.

27. Lin LY, Lee JH, Hong CE, Yoo GH and Advani SG. Preparation and characterization of layered silicate/glass fiber/epoxy hybrid nanocomposites via vacuum-assisted resin transfer molding (VARTM). *Compos Sci Technol* 2006; 66(13): 2116–2125.

28. Subramaniyan AK and Sun CT. Enhancing compressive strength of unidirectional polymeric composites using nanoclay. *Compos A Appl Sci Manuf* 2006; 37(12): 2257–2268.

29. Siddiqui NA, Woo RSC, Kim JK, Leung CCK and Munir A. Mode I interlaminar fracture behavior and mechanical properties of CFRPs with nanoclay-filled epoxy matrix. *Compos A Appl Sci Manuf* 2007; 38(2): 449–460.

30. Kornmann X, Rees M, Thomann Y, Necola A, Barbezat M and Thomann R. Epoxy-layered silicate nanocomposites as matrix in glass fibre-reinforced composites. *Compos Sci Technol* 2005; 65(14): 2259–2268.

31. Vlasveld DPN, Bersee HEN and Picken SJ. Nanocomposite matrix for increased fibre composite strength. *Polymer* 2005; 46(23): 10269–10278.

32. Vlasveld DPN, Daud W, Bersee HEN and Picken SJ. Continuous fibre composites with a nanocomposite matrix: Improvement of flexural and compressive strength at elevated temperatures. *Compos A Appl Sci Manuf* 2007; 38(3): 730–738.

33. Carroll BJ. The accurate measurement of contact angle, phase contact areas, drop volume, and Laplace excess pressure in drop-on-fiber systems. *J Coll Interface Sci* 1976; 57(3): 488–495.

34. Cassagnau P. Melt rheology of organoclay and fumed silica nanocomposites. *Polymer* 2008; 49: 2183–2196.

35. Renger C, Kuschel P, Kristoffersson A, Clauss B, Oppermann W and Sigmund W. Rheology studies on highly filled nano-zirconia suspensions. *J Eur Ceramic Soc* 2007; 27: 2361–2367.

36. Sarvestani AS. Modelling the solid-like behaviour of entangled polymer nanocomposites at low frequency regimes. *Eur Polymer J* 2008; 44: 263–269.

37. Sepehr M, Utracki A, Zheng X and Wilkie CA. Polystyrenes with macro-intercalated organoclay. Part II. *Rheology Mech Perf Polymer* 2005; 46: 11569–11581.

38. Dorigato A, Pegoretti A and Penati A. Linear low-density polyethylene – silica micro- and nanocomposites: Dynamic rheological measurements and modeling. *Exp Polymer Lett* 2010; 4(2): 115–129.

39. Brouwer WD, van Herpt ECFC and Labordus M. Vacuum injection moulding for large structural applications. *Compos Part A* 2003; 34: 551–558.

40. Strong AB. *Fundamentals of composites manufacturing*. Dearborn, MI: Society of Manufacturing Engineers, 2008.

41. Quaresimin M. private communication, 2009.

42. Ke Y, Lu J, Yi X, Zhao J and Qi Z. The effects of promoter and curing process on exfoliation behavior of epoxy/clay nanocomposites. *J Appl Polymer Sci* 2000; 78: 808–815.

43. Abdel-Goad M and Potschke P. Rheological chracterization of melt processed polycarbonate-multiwalled carbon nanotube composites. *J Non-Newtonian Fluid Mech* 2005; 128: 2–6.

44. Akbari B and Bagheri R. Deformation mechanism of epoxy/clay nanocomposite. *Eur Polymer J* 2007; 43: 782–788.

45. Basara C, Yilmazer U and Bayram G. Synthesis and characterization of epoxy based nanocomposites. *J Appl Polymer Sci* 2005; 98: 1081–1086.

46. Benfarhi S, Decker C, Keller L and Zahouily K. Synthesis of clay nanocomposite materials by light-induced crosslinking polymerization. *Eur Polymer J* 2004; 40: 493–501.

47. Dean D, Walker R, Theodore M, Hampton E and Nyairo E. Chemorheology and properties of epoxy/layered silicate nanocomposites. *Polymer* 2005; 46: 3014–3021.

48. Zunjarrao SC, Sriraman R and Singh RP. Effect of processing parameters and clay volume fraction on the mechanical properties of epoxy-clay nanocomposites. *J Mater Sci* 2006; 41: 2219–2228.

49. Mohan TP, Kumar MR and Velmurugan R. Mechanical and barrier properties of epoxy polymer filled with nano-layered silicate clay particles. *J Mater Sci* 2006; 41: 2929–2937.

50. Kinloch AJ and Taylor AC. The mechanical properties and fracture behaviour of epoxy-inorganic micro- and nano-composites. *J Mater Sci* 2006; 41: 3271–3297.

51. Yasmin A, Abot JL and Daniel IM. Processing of clay/epoxy nanocomposites by shear mixing. *Scripta Materialia* 2003; 49: 81–86.

52. Jia QM, Zheng M, Xu CZ and Chen HX. The mechanical properties and tribological behavior of epoxy resin composites modified by different shape nanofillers. *Polymers Adv Technol* 2006; 17: 168–173.

53. Dorigato A, Pegoretti A, Bondioli F and Messori M. Improving epoxy adhesives with zirconia nanoparticles. *Compos Interf* 2010; 17: 873–892.

54. Gao SL, Mader E and Plonka R. Nanocomposite coatings for healing surface defects of glass fibers and improving interfacial adhesion. *Compos Sci Technol* 2008; 68(14): 2892–2901.

55. Vlasveld DPN, Parlevliet PP, Bersee HEN and Picken SJ. Fibre-matrix adhesion in glass-fibre reinforced polyamide-6 silicate nanocomposites. *Compos A Appl Sci Manuf* 2005; 36(1): 1–11.

56. Park JM, Wang ZJ, Jang JH, Gnidakoung JRN, Lee WI, Park JK, et al. Interfacial and hydrophobic evaluation of glass fiber/CNT-epoxy nanocomposites using electro-micromechanical technique and wettability test. *Compos A Appl Sci Manuf* 2009; 40(11): 1722–1731.

57. Bozkurt E, Kaya E and Tanoglu M. Mechanical and thermal behavior of non-crimp glass fiber reinforced layered clay/epoxy nanocomposites. *Compos Sci Technol* 2007; 67(15–16): 3394–3403.

58. Haque A and Shamsuzzoha M. S2-glass/epoxy polymer nanocomposites:Manufacturing, structures, thermal and mechanical properties. *J Compos Mater* 2003; 37(20): 1821–1837.